Characterization of the zebrafish mutant *ahr2*^{hu3335}

Grétar Guðmundsson

Líf- og umhverfisvísindadeild
Háskóli Íslands
2016

Characterization of the zebrafish mutant *ahr2*^{hu3335}

Grétar Guðmundsson

15 eininga ritgerð sem er hluti af
Baccalaureus Scientiarum gráðu í Sameindalíffræði

Leiðbeinendur
Zophonías O. Jónsson
Valerie H. Maier

Líf- og umhverfisvísindadeild
Verkfræði- og náttúruvísindasvið
Háskóli Íslands
Reykjavík, Maí 2016

Characterization of the zebrafish mutant *ahr2*^{hu3335}
15 eininga ritgerð sem er hluti af *Baccalaureus Scientiarum* gráðu í Sameindalíffræði

Líf- og umhverfisvísindadeild
Verkfræði- og náttúruvísindasvið
Háskóli Íslands
Askja, Sturlugötu 7
101 Reykjavík

Sími: 525 4000

Skráningarupplýsingar:
Grétar Guðmundsson, 2016, *Characterization of the zebrafish mutant ahr2*^{hu3335}, BS ritgerð, Líf- og umhverfisvísindadeild, Háskóli Íslands, 21 bls.

Prentun: Háskólaprent
Reykjavík, Maí 2016

Útdráttur

Arýl kolvatnsefnis viðtakinn (AHR) er bindil virkjaður umritunarþáttur og er almennt þekktur fyrir að miðla viðbrögðum við eiturefnum í umhverfi t.d. dioxin (TCDD; 2,3,7,8 – tetrachlorodibenzo-[p]-dioxin). Eigi að síður, benda nýjustu rannsókir til að AHR hafi hlutverk í ýmsum fleiri líffræðilegum ferlum. Sebrafiska stökkbrigðið *ahr2*^{hu3335} sýnir verulegar breytingar í stærð og lagi á beineiningum í höfði, m.a. grennra höfuð og útstæðari neðri kjáka. Í þessu verkefni var gerð tilraun til að rannsaka frekar þær breytingar í lögun höfuðbeina sem *ahr2*^{hu3335} stökkbreytingin veldur með rúmfræðilegri formgreiningu (e. geometric morphometrics) á sebrafiskafóstrum 5 dögum eftir frjóvgun (5 dpf). Auk þess var tjáning nokkurra markgena skoðuð fyrir AHR með RT-qPCR á þrem ólíkum stigum þroskunar (3, 4 og 5 dpf). Rúmfræðileg formgreining greinir breytingar á lögun beineininga í höfði líklega tengdar bæði *ahr2*^{hu3335} stökkbreytingu og genatískum bakgrunn sebrafiskasýna. Engar marktækar breytingar fundust á tjáningu markgena. Frekari rannsóknir á *ahr2*^{hu3335} stökkbrygðinu eru áhugaverðar svo hægt sé að skilja betur hlutverk AHR í að skilgreina svipgerðareinkenni höfðubeina og í öðrum lífeðlisfræðilegum ferlum.

Abstract

The Aryl hydrocarbon receptor (AHR) is a ligand-activated transcription factor and is commonly known to mediate xenobiotic responses to environmental toxins e.g. dioxin (TCDD; 2,3,7,8–tetrachlorodibenzo-[p]-dioxin). However, an increasing amount of experimental evidence suggest AHR also has a role in a variety of biological processes. The zebrafish mutant *ahr2*^{hu3335} shows radical changes in the size and shape craniofacial elements, including a narrowing of the head and increased protrusion of the lower jaw. In this project, an effort was made to further investigate shape changes of the pharyngeal skeleton associated with the *ahr2*^{hu3335} mutation by applying geometric morphometric on zebrafish embryos at 5 days post fertilization (dpf). Additionally, expression of several known AHR gene targets was examined using real-time qPCR at three different stages of development (3, 4 and 5 dpf). Morphological analyses detect shape changes in craniofacial elements likely associated with both the *ahr2*^{hu3335} mutation and the genetic background of the zebrafish strains. No significant up or down regulation of AHR target genes was detected in the expression analysis. Further study of the zebrafish mutant *ahr2*^{hu3335} presents a great opportunity to decipher the role of the AHR in defining craniofacial features and other physiological processes.

Fyrir Heklu og Sögu

Table of contents

List of figures

List of tables

Abbreviations

AHR/AhR: Aryl hydrocarbon receptor

ARNT: Aryl hydrocarbon nuclear translocator

BHLB: Beta (β)-helix-loop-helix

BNF: β-Naphthoflavone

CNC: Cranial neural crest

CV: Canonical variate

CVA: Canonical variate analysis

Dpf: Days post fertilization

Hsp90: Heat shock protein 90

NES: Nuclear export signal

NLS: Nuclear location signal

NTC: Non-template control

PC: Principal component

PCA: Principal component analysis

PCR: Polymerase chain reaction

PFA: Paraformaldehyde

RT-qPCR: Real-time quantitative polymerase chain reaction

TILLING: Targeting Induced Local Lesions in Genomes

TCDD: 2,3,7,8 -Tetrachlorodibenzo-*p*-dioxin

XAP2: X-associated protein 2

XRE: Xenobiotic regulatory element

Acknowledgements

First I would like to thank Zophanías O. Jónsson for giving me the chance to work on this project and for reviewing this essay. A special thanks go to Valerie H. Maier for her exceptional assistance, guidance and valuable advice. I am grateful to Kalina Kapralova for all her advice and genuinely helpful comments. I would also like to thank all those working at the zebrafish research facilities in the University of Reykjavík for making me always feel welcome and Sævar Ingþórsson for his assistance with the microscope in Læknagarður.

1 Introduction

1.1 The Aryl hydrocarbon receptor

The Aryl hydrocarbon receptor (AHR) is a ligand activated transcription factor and is best known for mediating xenobiotic responses to various environmental toxins, such as dioxin (TCDD; 2,3,7,8 – tetrachlorodibenzo-[p]-dioxin) (Barouki et al. 2007). However, increasing experimental evidence suggests AHR involvement in various physiological and endogenous processes, such as cell cycle control, (cell adhesion and migration), tumor development, reproductive processes, hematopoiesis and immune system homeostasis (Goodale et al. 2012; Barouki et al. 2007). Also more recently, in addition to sensing xenobiotics, AHR has been found to bind bacterial pigments in regulation of antibacterial defense (Moura-Alves et al. 2014).

AHR belongs to the basic helix-loop-helix (bHLH-PAS) superfamily of proteins. The bHLH binds the aryl hydrocarbon responsive elements (AHREs) and the PAS domain includes the ligand binding domain and facilitates dimerization and interactions with other proteins. The primary ligands for AHR are polycyclic or halogenated aromatic hydrocarbons (PAHs and HAHs), for example TCDD, β-Naphthoflavone and leflunomide (Gerger et al. 2014; Goodale et al. 2012) (*Figure 1.1*). Currently, no definitive endogenous ligands are known for AHR. However some molecules have attained interest as potential endogenous ligands and participants in endogenous AHR function, such as the tryptophan degradation products kynurenines and 6-formylindolo[3,2-b] carbazole (FICZ) (Jönson et al. 2010; Wincent et al. 2016). Nevertheless, the search for endogenous ligands for the AHR is still ongoing (Nguyen, Linh P. 2008)

AHR binding to TCDD and resulting expression of certain isoforms of cytochrome P450 (among other enzymes and transporters) is a typical example of the AHR pathway (Barouki et al. 2007) (*Figure 1.2*). The AHR resides in the cytosol in a complex with hsp90, XAP2 and p23 and possibly other proteins. Subsequent to ligand binding, AHR disassociates from its cytoplasmic protein complex. This in turn, exposes the NLS of the bHLH domain, facilitating migration into the nucleus. Once inside the nucleus, AHR becomes a functional transcription factor by heterodimerizing with aryl hydrocarbon nuclear translocator (ARNT). By associations with different co-repressors and co-activators, the heterodimer affects transcription of target genes via upstream promotor regions. Transcriptional regulation terminates with AHR disassociation from ARNT and DNA. Subsequently, exportins bind the ELS, and AHR is exported to the cytosol, where it is degraded in the proteasome (Barouki et al. 2007).

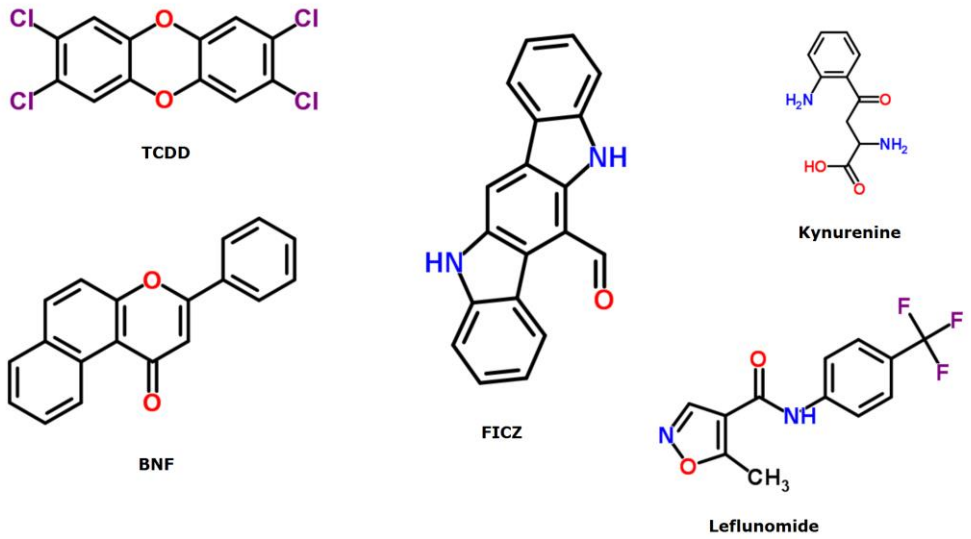

Figure 1.1 *– Examples of AHR ligands. Still no definitive endogenous ligands are known for AHR. Abbreviations: BNF, β-Naphthoflavone; TCDD, 2,3,7,8 -Tetrachlorodibenzo-p-dioxin; FICZ, 6-Formylindolo(3,2-b)carbazole.*

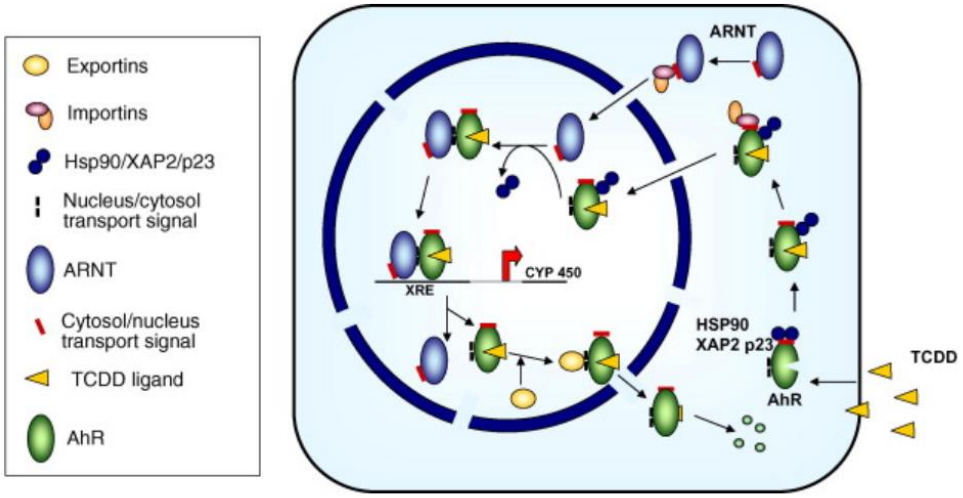

Figure 1.2 - *Transcriptional activation by AHR. Binding of AHR ligands (e.g. TCDD) releases the Hsp90/XAP2/p23 complex from AHR, exposing the NLS and allowing the binding of importins to the receptor and subsequent translocation into the nucleus. Inside AHR sheds the Hsp90/XAP2/p23 complex and hetero-dimerizes with ARNT. The dimer can then act as a transcription factor, binding to consensus regulatory elements (XREs) and facilitating expression of genes such as CYP 450. Afterwards AHR is exported into the cytosol via exportins and degraded in the proteasome.* (*Figure adopted from Barouki, Coumoul, & Fernandez-Salguero, 2007).*

The AHR shows high evolutionary conservation across animal phyla (Hahn 2002). The receptor is present in at least three invertebrate phyla and phylogenetic evidence suggests that AHR was present in early bilateral metazoans. However invertebrate AHR doesn't bind environmental toxins, suggesting an ancestral endogenous role for the AHR protein. There are three paralogues of AHR that currently have been identified in zebrafish, AHR1A, AHR1B and AHR2 (Andreasen et al. 2002; Karchner et al. 2005; Tanguay et al. 1999). AHR1A lacks a transactivation domain and does not bind either TCDD or BDF and even though AHR1B binds TCDD, it does so with a much lower affinity than AHR2. Thus AHR2 is the primary mediator of xenobiotic responses in zebrafish (Barouki et al. 2007; Hahn 2002). It is proposed that AHR isoforms originated from duplication of the AHR gene in the vertebrate linage and possibly led to the partitioning of AHR biological roles between isoforms in cartilaginous fishes (Hahn 2002).

A great opportunity to investigate these roles is presented by the zebrafish mutant *ahr2*^{hu3335} (Goodale et al. 2012). The mutant was produced by the TILLING (Targeting Induced Local Lesions in Genomes) method producing a point mutation in the *ahr2* gene. This results in a premature stop-codon upstream of the transactivation domain, allegedly resulting in an inactivated protein (*Figure 1.3*). Adult *ahr2*^{hu3335} mutants show jaw, gill and fin malformations in conjunction with some striking changes in skeletal structures of the skull (*Figure 1.4*).These findings indicate a role for the AHR in craniofacial development and other physiological processes in zebrafish.

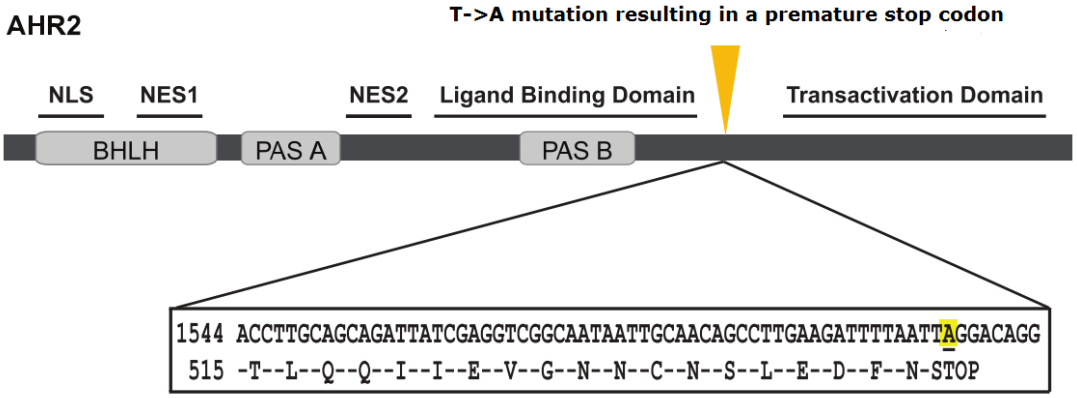

Figure 1.3 *– Schematic diagram of the AHR2 protein in ahr2*^{hu3335} *mutant zebrafish. ahr2*^{hu3335} *protein contains a point mutation in residue 534, leaving a premature stop codon and presumably resulting in an inactive AHR2 protein lacking a transactivation domain. NES: nuclear export signal, NLS: nuclear localization signal. BHLB: Beta (β)-helix-loop-helix. (Figure adopted from Goodale et al., 2012).*

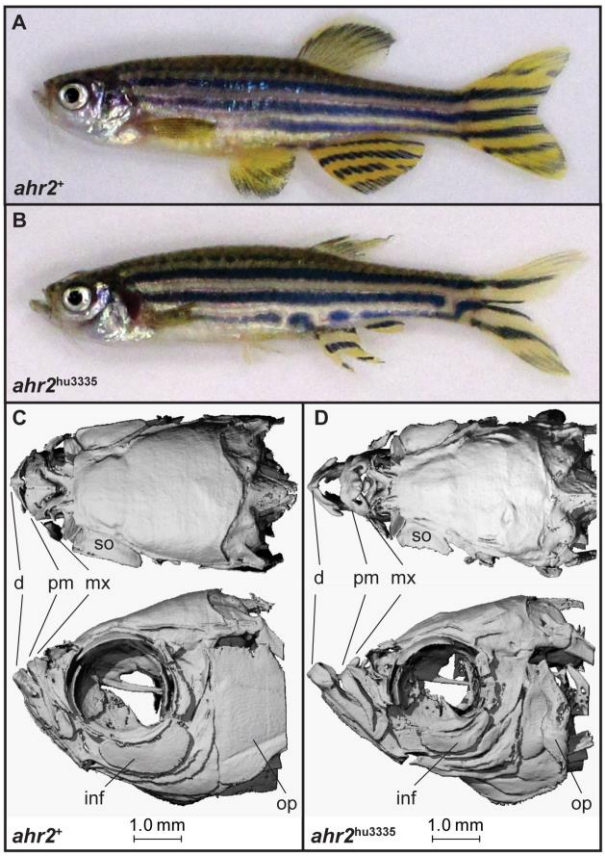

***Figure 1.4** – Ahr2^{hu3335} mutant shows radical changes in craniofacial bone structure. (A-B) Lateral view of adult wild type zebrafish (A) and mutant (B). Abnormalities in fin development were observed in ahr2^{hu3335}mutant. (C-D) Also, MicroCt scanning unveils alterations in various bone structures such as the dentate (d), premaxilla (pm), maxilla (mx), supraorbital (so), infraorbital 3(inf) and operculum. (Figure adopted from Goodale et al., 2012).*

1.2 Craniofacial development in zebrafish

Development of the vertebrate head skeleton comprises a complex series of events involving the cranial neural crest (CNC) and all three germ layers (endoderm, mesoderm and ectoderm) (Knight & Schilling 2000). These events lead to the formation of the three major regions of the vertebrate skull, the dermatocranium, neurocranium and splanchnocranium, The splanchnocranium consisting of the pharyngeal skeletal elements, exemplifies one of the most complex and diverse anatomical structures in vertebrate evolution. The pharyngeal skeleton is derived from CNC cells. In development, the CNC disassociate from the neural ectoderm, migrating laterally along the neural folds to form the pharyngeal skeletal elements (mandibular, hyoid and branchial arches) (*Figure 1.5*). Each of these structures, is derived from one of three distinct streams of CNC cell derived from different rostro-caudal segments of the developing neural tube (rhombomeres), with CNC homeotic gene expression defining segmental differences (Knight & Schilling 2000; C. Yelick & F. Schilling 2004). Fine changes in the patterning of the CNC are proposed to be integral to the large variation in shape and function of the pharyngeal head skeleton observed in vertebrates.

Supposedly, interconnected molecular signaling pathways are fundamental in defining cell behavior and patterning in development and resulting structural phenotypes. A recent study, looking at differential gene expression in four sympatric Artic charr morphs in the lake Tingvallarvatn (Iceland), found the receptor *ahr2b* to be an upstream transcription factor for a network of co-expressed genes with higher expression in benthic morphs (blunter snouts and more sub-terminal mouths) than limnetic morphs (pointier snouts and terminal mouth). Thus the study suggests the AHR pathway to be a key modulator in defining the shape of the craniofacial skeleton in development of Artic charr (Ahi et al. 2015). Interestingly, the general narrowing of the head and greater protrusion of the lower jaw of the zebrafish *ahr2*^{hu33335} mutant, shows some resemblance to the craniofacial phenotype of the limnetic Artic charr morph. In light of the highly conserved nature of the AHR it's not unlikely these observations have implications for the development of craniofacial features in other vertebrates.

In general, zebrafish have proven to be a valuable model to study the genetic underpinnings of craniofacial development and evolution of the vertebrate skull (Lindsey & Gage 2015; C. Yelick & F. Schilling 2004). In this project we further investigated the shape changes associated with the *ahr2*^{hu33335} mutation by applying geometric morphometrics to early larval stage craniofacial elements visualized by staining of cartilage. Additionally we looked at the expression of several AHR target genes at three larval stages of development, with previously observed AHR-mediated changes in expression in the zebrafish jaw primordium.

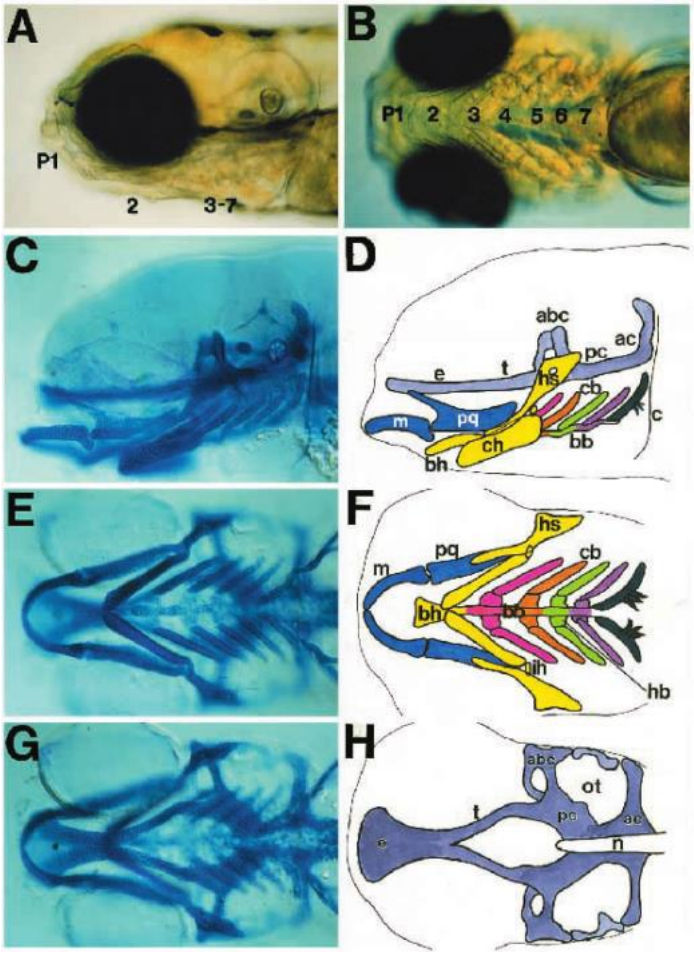

Figure 1.5 – *Craniofacial structures of wild type zebrafish larvae. (A-B) Lateral and ventral view of a live zebrafish embryo about 6 days old. The outline of the jaw and branchial arches were visible (P1-7). (C-H) Whole-mount Alcian blue stained embryos with corresponding diagrams showing the pharyngeal skeleton from both a lateral (C-D) and ventral view (E-H). Structures in diagrams have a matching color, the P1 (mandibular arch) is in blue, P2 (hyoid arch) is yellow, P3 (first branchial arch) is pink, P4 is orange, P5 is green, P6 is purple, P7 is black and the neurocranium (D, G-H) is grey. Diagram abbreviations: abc, anterior basicranial commissure; ac, auditory capsule; bb, basibranchial; bh, basihyal; c, cleithrum; cb, ceratobranchial; ch, ceratohyal; e, ethmoid plate; hb, hypobranchial; hs, hyosymplectic; ih, interhyal; m, Meckel's cartilage; n, notochord; ot, otic capsule; pc, parachordal; pq, palatoquadrate; t, trabeculae cranii. (Figure adopted from Piotrowski et al., 1996).*

2 Materials and methods

2.1 Fish stocks and sampling

Ten offspring of heterozygous crosses of mutant *ahr2*^{hu3335} zebrafish were obtained from Dr. Pedro Alves at Max Planck Institute for Infection Biology. The zebrafish were retained at the zebrafish research facilities of the University of Reykjavík and used to produce embryos for analysis. DNA was isolated from caudal fin clips from the 10 individuals, and the AHR2 gene was PCR amplified and analyzed using agarose gel electrophoresis (see *Figure A.1* in appendix). The PCR products were genotyped with Sanger sequencing (by Beckman Coulter Genomics). The sequencing results indicated that 5 of the 10 fish were heterozygotes, of which one was female. Four of the remaining fish were wild type and 1 was a homozygous mutant. The *ahr2*^{hu3335} homozygous fish was malformed and died before reaching maturity. By crossing the female heterozygote with a heterozygous male, a mixture of genotypes was produced (including an estimated 25% of *ahr2*^{hu3335} homozygotes and 50 % *ahr2*^{hu3335} heterozygotes assuming Mendelian inheritance). Optimally the genotypes would be segregated into distinct groups but due to lack of homozygous mutants to cross this was not feasible for this project. Thus, the offspring derived from heterozygote crossings were called *ahr2*^{hu3335} HC and were sampled 3, 4 and 5 days post fertilization (dpf) and used for further analyses.

As control group, crosses from individuals not bearing the *ahr2*^{hu3335} mutation, as indicated from sequencing results, were called *ahr2*^{hu3335} WT (referring to wild type embryos being derived from *ahr2*^{hu3335} heterozygous crossing). Additionally, an external wild type strain (called WT) was used as a second control group to detect any differences due to genetic background.

2.2 Staining and photographing

In order to visualize the craniofacial structure of zebrafish embryos during development, samples were stained for cartilage (Alcian blue) and bone (Alizarin red) at 3, 4 and 5 dpf. For each biological group and larval stage, embryos were fixed in 4% paraformaldehyde (PFA) solution. The double-acid free-staining protocol was modified from (Walker & Kimmel 2007).

In total, 127 embryos were stained and photographed (of which 98 were 5 dpf). For photographing, embryos were fixed in 85% glycerol solution on a microscope slide and photographed ventrally using a Leica (DMI3000 B) inverted microscope and with the same magnification for all samples. A maneuverable cover slide, elevated over fixed embryos (using additional microscope slides), was used to position embryos correctly for photographing.

2.3 Geometric morphometrics

Twelve landmarks positioned on anatomical features such as the ethmoid plate (indicative of the position of the upper jaw) and lower jaw were selected to assess possible differences

in the structure of the craniofacial elements of the developing head of the *ahr2*^{hu3335} mutant *(Figure 2.1).* Landmarks were digitized for 75 photographed embryos using tps.DIG2 (Rohlf, 2006). A total of 15 digitized samples, showing lack of symmetry due to malformations or unfavorable orientation were excluded, leaving 60 for the following analyses. Mor-phoJ (Klingenberg, 2011) was then used for Generalized Procrustes analysis (GPA). Only the symmetric component of variance was used for further analysis. Size-dependent variation (allometry) was accounted for by using the residuals from regression of shape (symmetric component of variation) on centroid size for all the analyses.

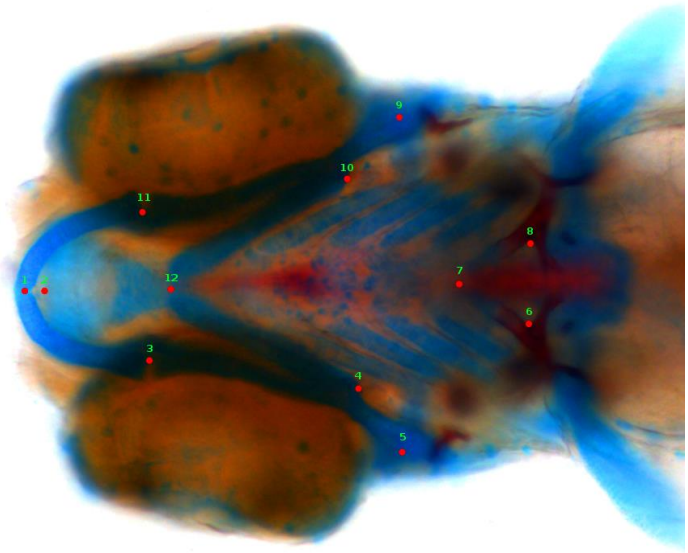

***Figure 2.1** – Assigned landmarks for geometric morphometrics on a 5 dpf zebrafish head. Landmarks were chosen to describe relative positions of different skeletal structures in the head and its overall shape. Three centroid and 9 symmetric landmarks were assigned as follows: (1) The symphysis of the left and right Meckel's cartilage; (2) Center tip of the ethmoid plate; (3 and 11) Meckel's cartilage and palatoquadrate joint; (4 and 10) Distal end of the posterior hyoid arches; (5 and 9) center of hyosymplectic; (6 and 8) Branching of P7 branchial arch and their teeth; (7) Joining of anterior p7 branchial arches; (12) Joining of anterior hyoid arches.*

2.4 RNA extraction and cDNA synthesis

For expression analysis 3, 4 and 5 dpf zebrafish embryos were sampled in RNAlater (Ambion) and stored at -20 °C. To extract RNA, Trizol Reagent protocol from Life technologies (MAN0001271) was adopted using a homogenate of 50 embryos (40 for second biological replicate). Embryos were homogenated with a disposable Kontes Pellet Pestle Cordless Motor tissue grinder (Kimble Kontes). For phase separation 4-bromochloropropan was used instead of chloroform. RNA was treated with DNase (New England Biolabs) to remove contaminating DNA. Quantity of RNA was assessed using a NanoDrop ND-1000 UV/Vis-Spectrophotometer (NanoDrop). RNA was reverse transcribed to cDNA using Superscript 2 reverse transcriptase (Invitrogen) with random

hexamers and 1000 ng of RNA for each reaction. For each biological replicate samples were prepared without reverse transcriptase (-RT) to test for genomic DNA contamination.

2.5 Real-time quantitative PCR and analysis of expression data

Real-time quantitative PCR was performed in 96 well PCR-plates on an ABI 7500 real-time PCR System (Applied Biosystems) using Maxima SYBR green (Thermo Fisher scientific). Biological replicates were run in a duplicate with a non-template control (NTC). The RT-qPCR was run with a 2 min hold at 50 °C and a 10 min hot start at 95 °C followed by the amplification step for 40 cycles of 15 sec denaturation at 95 °C and 1 min annealing/extension at 60 °C. A dissociation step (60 °C–95 °C) was performed at the end of the amplification phase to identify a single, specific product for each primer set.

To analyze expression data, mean C_T values of technical duplicates were used from all samples. Target genes were normalized with reference gene *ppia2* (reference genes are discussed further in expression results), by calculating $\Delta C_{Ttarget} = C_{Ttarget}\text{-}C_{Treference}$. To normalize samples, the value $\Delta\Delta C_T$ was calculated ($\Delta\Delta C_T = \Delta C_{Ttarget} - \Delta C_{Tcalibrator}$). Finally, to visualize the data, the fold-difference (FD) in expression was calculated, as follows: $FD = 2^{-\Delta\Delta CT}$.

3 Results

3.1 Development and growth of the ventral pharyngeal skeleton in zebrafish

Embryos at hatching and early larval stages of development (2-5 dpf) were stained for bone and cartilage and photographed to produce a developmental series of craniofacial bone structure (*Figure 3.1*). No craniofacial cartilage formation was observed until the post-hatching stage of development 3dpf, where we could detect the formation of the neurocranium (including the ethmoid plate), mandibular arch, hyoid arch and the first two branchial arches (P3 and P4). Most of the visible cartilage structures have formed by 4 dpf, including the remaining pharyngeal arches (P4-P7) and basihyal, additionally showing ossification in the operculum, parasphenoid, P7 and the neural tube. This demonstrates rapid formation and growth of the jaw and pharyngeal skeletal elements over the developmental period. At 5 dpf further growth was evident, size reduction in yolk sac and increased robustness. Thus 5 dpf zebrafish were chosen for following morphometric analyses.

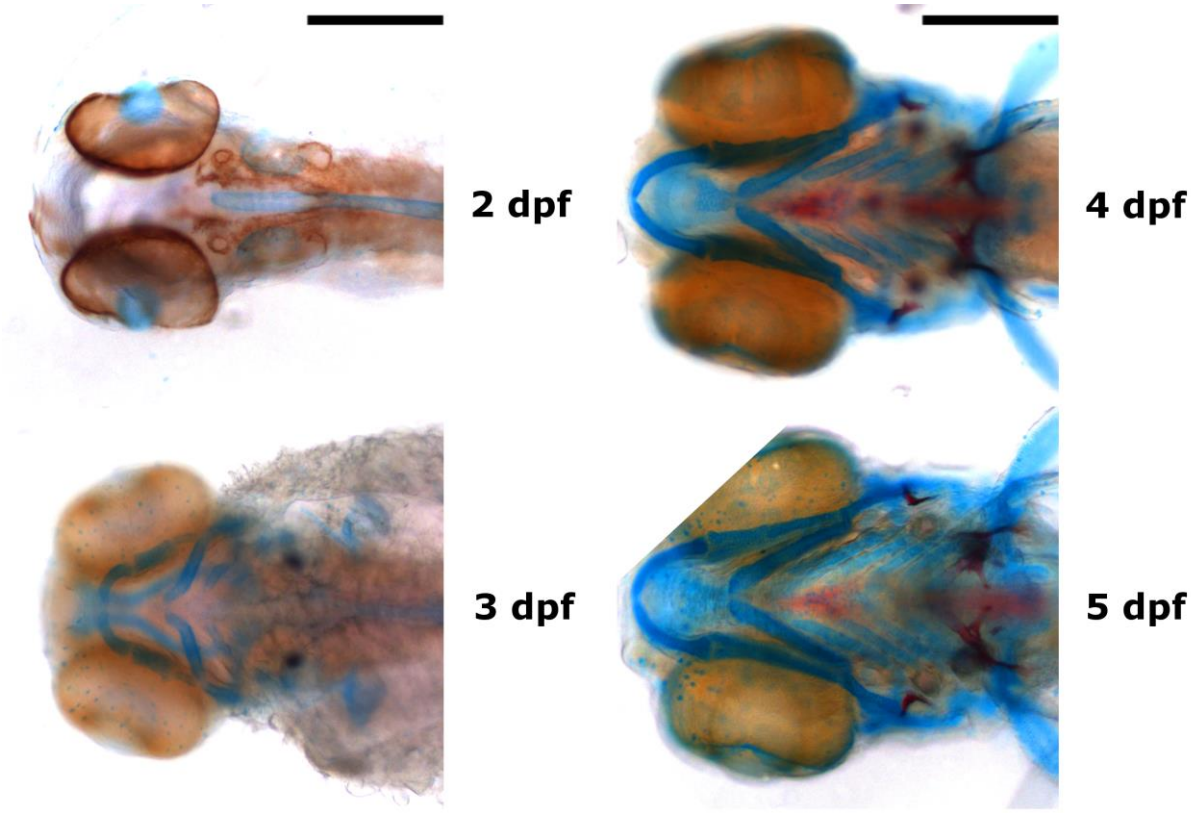

Figure 3.1 *– Development of craniofacial head structures of wild type zebrafish embryos (WT) 2-5 days post fertilization (dpf) seen from ventral side. Embryos were stained for cartilage (blue) and bone (red). Scale Bars = 25 µm.*

3.2 Geometric morphometrics

In order to correct for allometry (size-dependent variation), we looked at the regression of shape (symmetry component of variation) on centroid size (*Figure 3.2*). A permutation test against the null hypothesis of independence was performed, showing significant dependence between variables (p-value: 0,006). A size difference was noticeable in the ventral craniofacial skeleton of the zebrafish embryos between sample groups, with especially WT embryos being larger. Data points for *ahr2*^{hu3335} HC and *ahr2*^{hu3335} WT were more consistent, and only one sample in *ahr2*^{hu3335} WT showed unusually high centroid size. By using the regression residuals for the following analyses this observed size dependent variation was corrected for the following analyses.

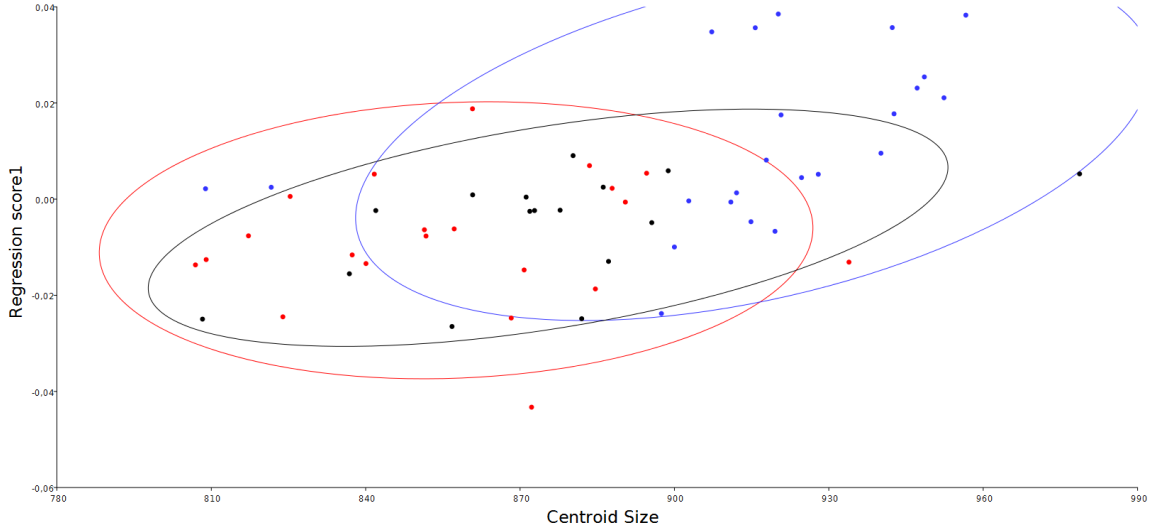

***Figure 3.2** – Regression of shape on centroid size for zebrafish embryos sampled 5 dpf. Data points are colored as follows: ahr2^{hu3335} HC, red; ahr2^{hu3335} WT, black; WT, blue. Confidence ellipses are set to 90%.*

Principal component analysis (PCA) gave some interesting insights into the shape change of the head skeletal elements that entailed the most variation (*Figure 3.3* and *Figure 3.4*). Principal component 1, 2 and 3 (PC1-PC3) explain 31,8 %, 24,6 % and 15,7 % of the variation, respectively. Overall, biological groups seemed to occupy a similar morphometric space for all three principal components with outliers present for all groups. A noticeable exception was *ahr2*^{hu3335} WT having generally higher PC1 loadings. The shape changes associated with this are a wider head and hyoid arch (*Figure 3.3*). Additionally, *ahr2*^{hu3335} HC appears to show a greater variation in PC1 and PC2 than control groups. However, *ahr2*^{hu3335} HC showed a lower variance for PC3 (higher values entailing a more elongated and protruding lower jaw) (*Figure 3.4*).

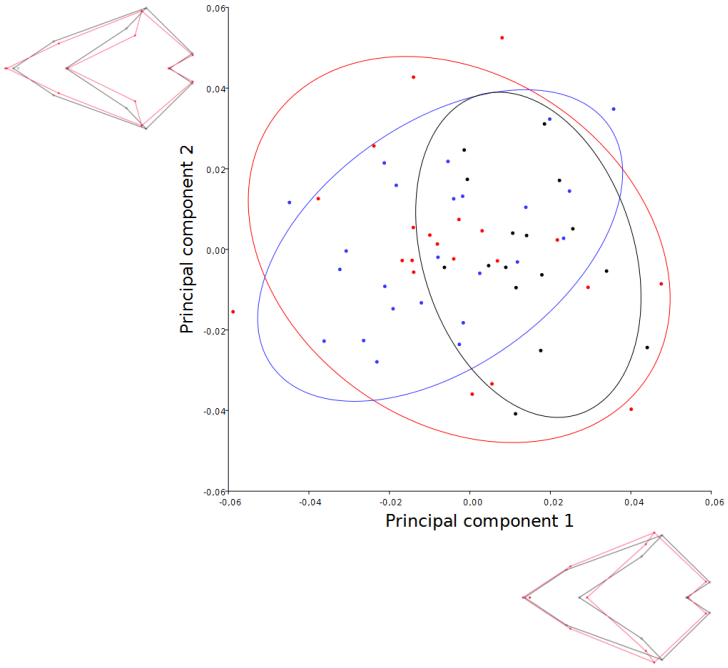

Figure 3.3 *– PCA scores shown in a scatter plot with the two principal components explaining the largest portion of the variation in the whole dataset. Allometry was corrected for by using regression residuals for PCA (see Figure 3.2).* Data points are colored as follows: *ahr2*^{hu3335} HC, red; *ahr2*^{hu3335} WT, black; WT, blue. *Confidence ellipses are set to 90%. Wireframe graphs show changes in Procrustes distance and were set to a scale factor of 0,1 and explain the morphological differences represented by each principal component, were red is a more extreme positive value and black a more extreme negative value.*

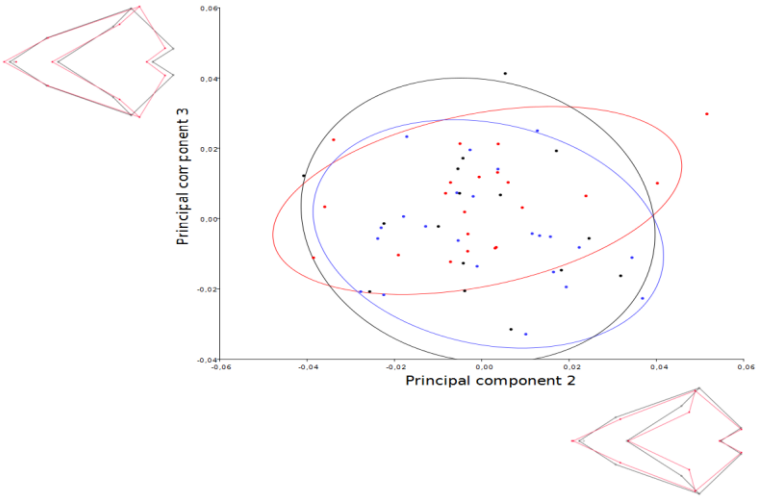

Figure 3.4 *- PCA scores shown in a scatter plot with the two principal components PC2 and PC3. Allometry was corrected for by using regression residuals for PCA (see Figure 3.2).* Data points are colored as follows: *ahr2*^{hu3335} HC, red; *ahr2*^{hu3335} WT, black; WT, blue. *Confidence ellipses are set to 90%. Wireframe graphs show changes in Procrustes distance and were set to a scale factor of 0,1 and explain the morphological differences represented by each principal component, were red is a more extreme positive value and black a more extreme negative value.*

To better understand the difference in shape of craniofacial elements between the different biological groups, a canonical variate analysis (CVA) was performed (*Figure 3.5*). Variation among groups was scaled by the inverse of the in-group variation producing canonical variate 1 and 2 (CV1 and CV2) defining 74,0 % and 26,0 % of the variation between groups, respectively. A significant difference is observed between all groups (p-value: *ahr2*^{hu3335} HC - WT, 0,0068; *ahr2*^{hu3335}HC – *ahr2*^{hu3335} WT, <0,0001; *ahr2*^{hu3335} WT – WT, <0,0001) with the greatest difference being between the two control groups (mostly associated with CV1). The shape changes associated with this were similar to what was observed in the PCA, notably that *ahr2*^{hu3335} WT has a wider head, narrower hyoid arch and slightly more protruding jaw than the WT. Nevertheless, a very interesting difference was seen between *ahr2*^{hu3335} HC and the two control groups in CV2, translating to a narrower head and more protruding jaw. A similar phenotype for the *ahr2*^{hu3335} mutant has previously been described in a study (as discussed in introduction) (Goodale et al. 2012). Interestingly, the *ahr2*^{hu3335} HC and *ahr2*^{hu3335} WT both differ from WT along CV1, indicating some mutual shape characteristics in *ahr2*^{hu3335} HC and *ahr2*^{hu3335} WT which are different from WT.

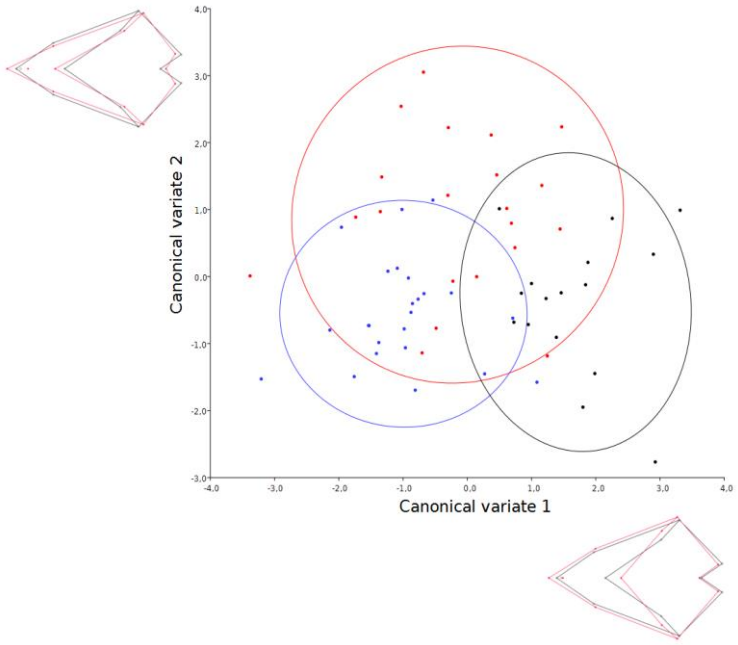

***Figure 3.5** – Scatter plot with CVA scores. Canonical variates Data points are colored as follows: ahr2*^{hu3335} *HC, red; ahr2*^{hu3335} *WT, black; WT, blue. Confidence ellipses are set to 90%. Wireframe graphs show changes in Procrustes distance and were set to scale factor 0,1 and explain the morphological differences represented by each canonical variate, were red is a more extreme positive value and black a more extreme negative value.*

3.3 Quantitative real-time PCR based analysis of expression

Two reference genes were chosen for a relative expression analysis, the widely used *Actb1,* coding for actin beta 1 and *ppia2 (peptidyl prolyl isomerase Aa),* which has been shown to be stably expressed in developing heads of zebrafish (Ahi et al. 2016). Three target genes were investigated with quantitative real-time expression analysis, sry-box containing gene 9b (*sox9b*), cytochrome P450A1 (*cyp1a1*) and forkhead box Q1 (*foxq1*). *Sox9b* is highly conserved across animal phyla, a major skeletal marker and downregulation via the AHR pathway has been associated with jaw malformations in zebrafish (Xiong et al. 2008). The well-known *cyp1a1* is a downstream target of the AHR pathway and is highly upregulated on AHR ligand dependent activation (Carney et al. 2004). Finally, *foxq1* is a forkhead box transcription factor with observed AHR-dependent upregulation in ventral craniofacial structures during zebrafish development (Planchart & Mattingly 2011).

To estimate the stability of the reference genes *actb1* and *ppia2* DNA amplification was plotted for measured developmental time points and biological groups (*Figure 3.6*). Higher amplification was detected in the control groups compared to *ahr2*^{hu3335} in the first replicate (*Figure 3.6A*) than in the second replicate (*Figure 3.6B*). However, a similar pattern of amplification was observed for both reference genes in the second biological replicate with a noticeable discrepancy seen in *ahr2*^{hu3335} WT compared to *ahr2*^{hu3335} HC and WT. Overall, a more stable amplification was seen for *ppia2* and together with the fact that *ppia2* has been observed to have a more stable expression in the developing head of zebrafish embryos than *actb1* (Ahi et al. 2016), *ppia2* was chosen as reference gene for the following relative expression analysis.

Target genes show noticeable differences in relative expression between the two biological replicates (*Figure 3.7*). Firstly and rather unexpectedly, *ahr2*^{hu3335} WT was measured with the lowest expression of *sox9b with ahr2*^{hu3335} HC having about 2-5 fold higher expression and WT having approximately ten-fold higher expression at the two later larval stages. Meanwhile, a much more stable expression was observed for the second replicate. Secondly, the expression of *cyp1a1* in *ahr2*^{hu3335} HC shows upregulation at 4 dpf, which was not seen in the second replicate. Lastly, all sample groups show upregulation of *cyp1a1* in the second replicate, while none is seen in the first replicate. Despite these discrepancies, both replicates show a similar or slightly lower expression of *cyp1a1* in *ahr2*^{hu3335} HC at 3 and 4 dpf. The gene expression of *foxq1* was investigated in the second biological replicate and shows stable expression, with less variance at later developmental stages.

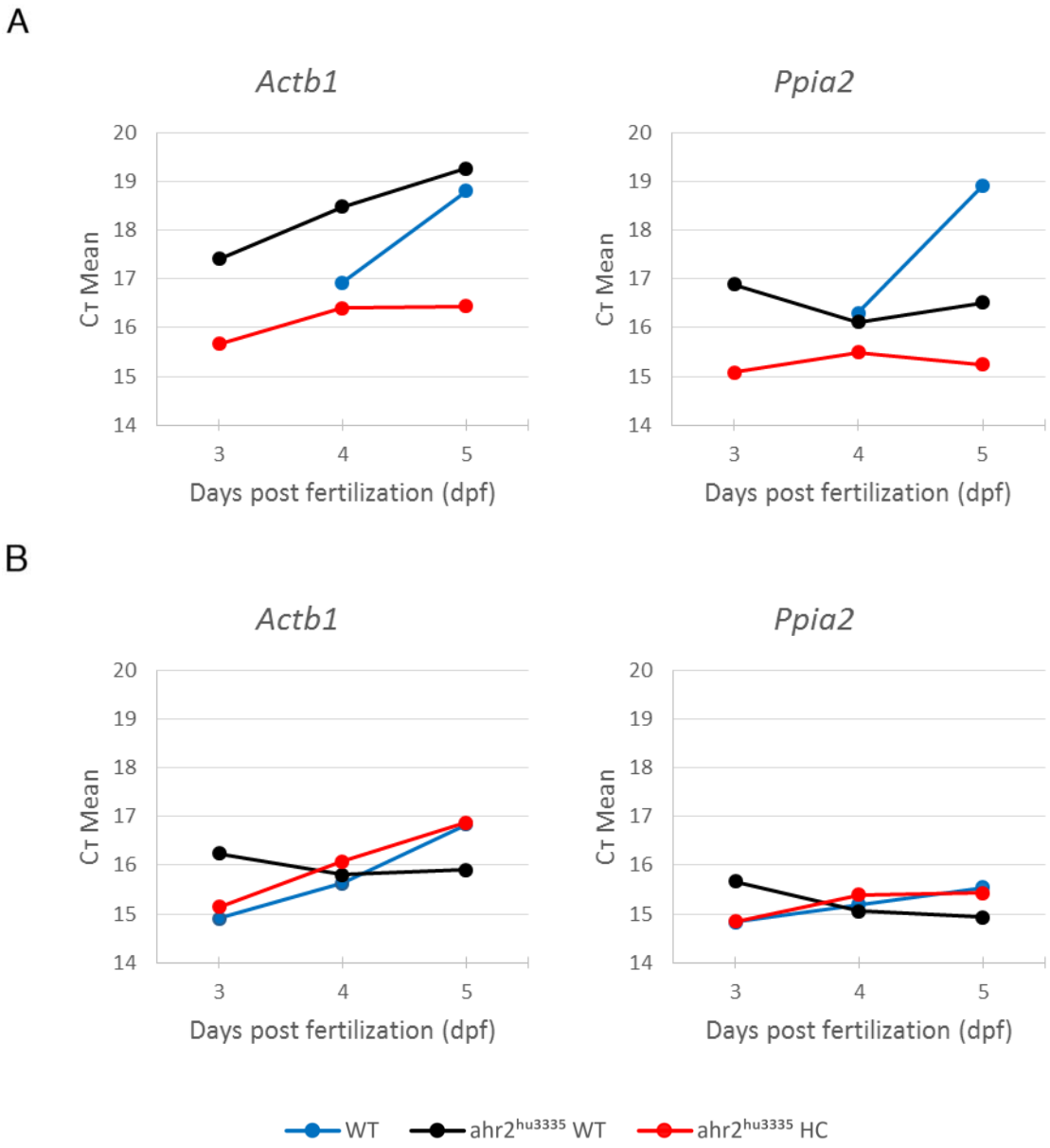

Figure 3.6 *– Amplification of reference genes actb1 and ppia2 in first (A) and second (B) biological replicate. WT 3dpf is excluded from the analysis of the first replicate.*

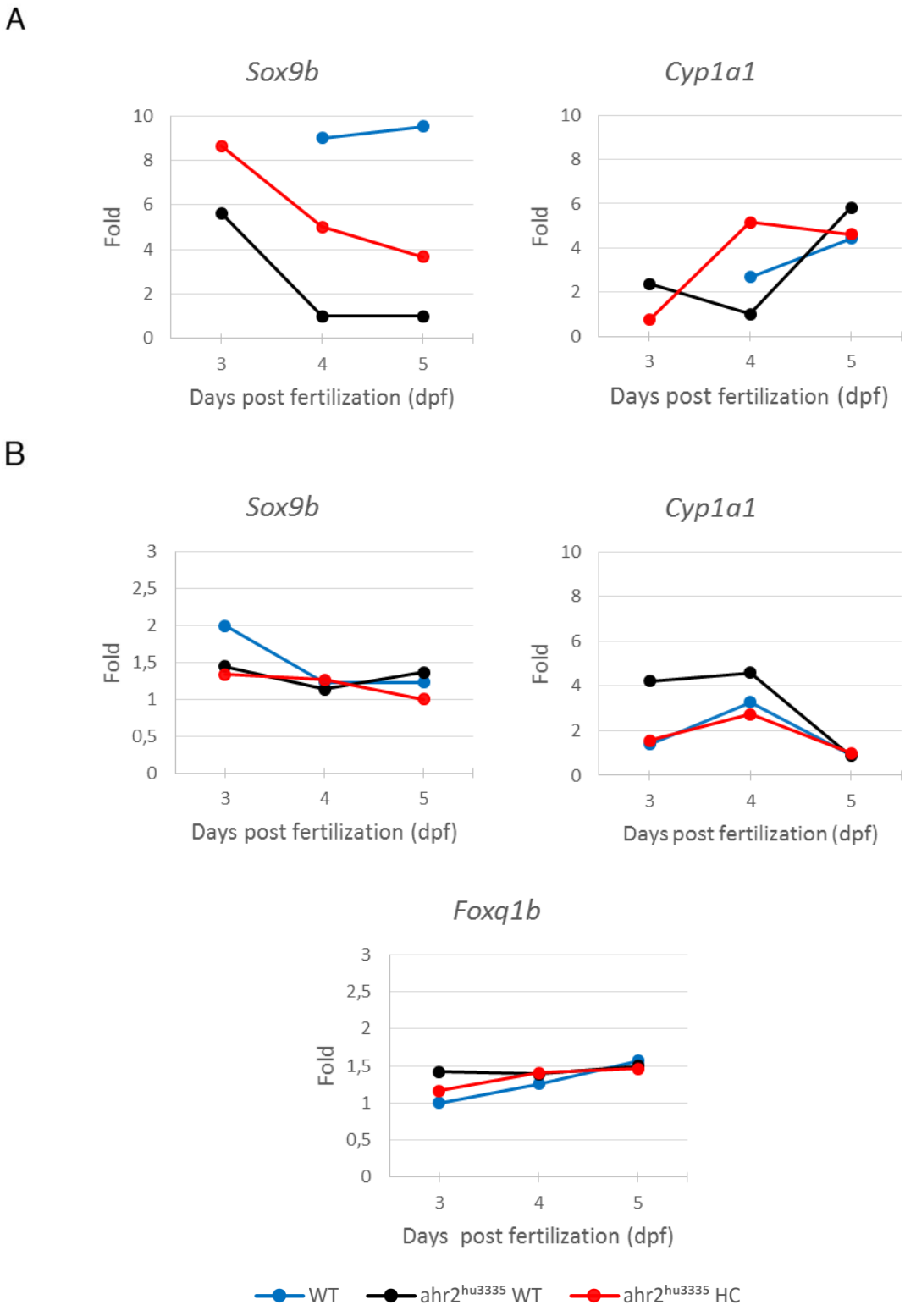

Figure 3.7 *– Relative expression of genes sox9b, cyp1a1 and foxq1b in whole zebrafish embryos at early larval stage of development. Ahr2^{hu3335} HC and control groups ahr2^{hu3335} WT and WT were compared at 3, 4 and 5 dpf using a homogenate of 30 embryos for each sample. First (A) and second (B) biological replicate for sox9b and cyp1a1 are shown, with additional one biological replicate for foxq1 expression. Samples used for calibration (A) ahr2^{hu3335} WT 4 dpf and (B) Ahr2^{hu3335} HC 5 dpf. WT 3dpf is excluded from the analysis in first replicate.*

4 Discussion

Morphometric analyses presented in this project show a number of interesting observations. Curiously, a substantial amount of shape variation was present between both control groups, clearly observed in the CVA (*Figure 3.5*), showing that *ahr2*^{hu3335} WT had a generally wider head, narrower hyoid arches and more protruding jaw than WT. A related observation of craniofacial shape difference between the groups was explained by PC1 (*Figure 3.3*). There could be several explanations for this perceived shape changes. For example *ahr2*^{hu3335} HC and *ahr2*^{hu3335} WT are of a similar genetic background, whereas WT originate from a different zebrafish stock. The possibility that differences in genetic background may be partly responsible for the divergence in head shape is further supported by the CVA, notably that some mutual shape characteristics in *ahr2*^{hu3335} HC and *ahr2*^{hu3335} WT were different from WT. Other possible explanations are slight differences in experimental procedure and arbitrary variation due to small sample size. It has to be noted that regardless of the small sample size and different genetic backgrounds, a significant difference was observed in pharyngeal skeleton shape of *ahr2*^{hu3335} HC compared to both control groups along CV2, conforming to the previously observed phenotype of the *ahr2*^{hu3335} zebrafish mutant (Goodale et al. 2012), namely narrowing of the head and protrusion of the lower jaw. Investigating this further using more biological groups with distinct genotypes and larger sample sizes would likely give clearer results. Collectively, these results demonstrate the strength of geometric morphometrics in detecting discrete changes in structural phenotypes despite small sample sizes.

Expression results do not seem to demonstrate any predicted trend of either down or upregulation of target genes over the observed larval stages of development. Discrepancies in the two biological replicates show the need for more expression data in order to get conclusive results. On the other hand, as evident by more stable amplification of reference genes and the more modest variation in target gene expression in the second biological replicate, it probably is a better representation of actual expression in the zebrafish embryos. Be that as it may, detecting variation in expression due to the *ahr2*^{hu3335} mutant is not a given fact. The likelihood of detecting such variation is greatly diminished as a result of two obvious caveats in the presented expression analyses. Firstly, using a group containing a mixture of genotypes (*ahr2*^{hu3335} HC) instead of groups of single established genotypes (such as homozygotes or heterozygotes for the mutant gene), lessens any observed effect owing to the mutation. Secondly, investigating expression in whole embryos rather than a more distinctly in the zebrafish head, probably lessens the chances of detecting any differences between mutant and control groups. Furthermore, the analysis represent expression in a wide range of organs and tissues that can display a widely different changes in expression than is present in the developing head (Xiong et al. 2008). Still, after correcting for these caveats, investigating further the expression of genes affecting craniofacial characteristics in the *ahr2*^{hu3335} zebrafish mutant presents an interesting area of study.

References

Ahi, E.P. et al., 2015. Differential expression of the aryl hydrocarbon receptor pathway associates with craniofacial polymorphism in sympatric Arctic charr. *EvoDevo*, 6(1), p.27. Available at: http://www.evodevojournal.com/content/6/1/27.

Ahi, E.P. et al., 2016. Effects of low levels of estrogen on gene expression during zebrafish larval head development. *PeerJ*, pp.1–29.

Andreasen, E. a et al., 2002. The zebrafish (Danio rerio) aryl hydrocarbon receptor type 1 is a novel vertebrate receptor. *Molecular pharmacology*, 62(2), pp.234–249.

Barouki, R., Coumoul, X. & Fernandez-Salguero, P.M., 2007. The aryl hydrocarbon receptor, more than a xenobiotic-interacting protein. *FEBS Letters*, 581(19), pp.3608–3615.

C. Yelick, P. & F. Schilling, T., 2004. Molecular dissection of craniofacial development using zebrafish. *Crit Rev Oral Biol Med*, 13(4), pp.308–322.

Carney, S.A., Peterson, R.E. & Heideman, W., 2004. 2,3,7,8-Tetrachlorodibenzo-p-dioxin Activation of the Aryl Hydrocarbon Receptor/Aryl Hydrocarbon Receptor Nuclear Translocator Pathway Causes Developmental Toxicity through a CYP1A-Independent Mechanism in Zebrafish. *Mol Pharmacol*, 66(3), pp.512–521.

Gerger, C.J. et al., 2014. Acute effects of β-naphthoflavone on cardiorespiratory function and metabolism in adult zebrafish (Danio rerio). *Fish Physiology and Biochemistry*, 41(1), pp.289–298.

Goodale, B.C. et al., 2012. AHR2 mutant reveals functional diversity of aryl hydrocarbon receptors in zebrafish. *PLoS ONE*, 7(1).

Hahn, M.E., 2002. Aryl hydrocarbon receptors : diversity and evolution 1. *Chemico-Biological Interactions*, 141, pp.131– 160.

Jönson, M.E. et al., 2010. The tryptophan photoproduct 6-formylindolo[3,2-b]carbazole (FICZ) binds multiple AHRs and induces multiple CYP1 genes via AHR2 in zebrafish. *Chem Biol Interact.*, 181(3), pp.447–454.

Karchner, S.I., Franks, D.G. & Hahn, M.E., 2005. AHR1B, a new functional aryl hydrocarbon receptor in zebrafish: tandem arrangement of ahr1b and ahr2 genes. *The Biochemical journal*, 392(Pt 1), pp.153–161.

Knight, R.D. & Schilling, T.F., 2000. Cranial Neural Crest and Development of the Head Skeleton Specification and Migration of the Skeletogenic CNC. *Landes Bioscience*, pp.1–12.

Lindsey, M. & Gage, C., 2015. Zebrafish Craniofacial Development: A Window into Early Patterning. *Curr Top Dev Biol*, 8(12), pp.1699–1712.

Moura-Alves, P. et al., 2014. AhR sensing of bacterial pigments regulates antibacterial defence. *Nature*, 512(7515), pp.387–392.

Nguyen, Linh P., C.A.B., 2008. The Search for Endogenous Activators of the Aryl Hydrocarbon Receptor. *Chem Res Toxicol*, 21(1), pp.102–116.

Piotrowski, T. et al., 1996. Jaw and branchial arch mutants in zebrafish I: anterior arches and cartilage differentiation. *Development (Cambridge, England)*, 123, pp.345–356.

Planchart, A. & Mattingly, C.J., 2011. 2,3,7,8-Tetrachlorodibenzo-p-dioxin Upregulates FoxQ1b in Zebrafish Jaw Primordium. *Chem Res Toxicol.*, 23(3), pp.480–487.

Rohlf FJ. 2006. “tpsDig, version 2.10.” http://life.bio.sunysb.edu/ morph/index.html.

Tanguay, R.L. et al., 1999. Cloning and characterization of the zebrafish (Danio rerio) aryl hydrocarbon receptor. *Biochim Biophys Acta*, 1444(1), pp.35–48. Available at: http://www.ncbi.nlm.nih.gov/entrez/query.fcgi?cmd=Retrieve&db=PubMed&dopt=Citation&list_uids=9931422.

Walker, M.B. & Kimmel, C.B., 2007. A two-color acid-free cartilage and bone stain for zebrafish larvae. *Biotechnic & histochemistry : official publication of the Biological Stain Commission*, 82(1), pp.23–28.

Wincent, E. et al., 2016. Biological effects of 6-formylindolo[3,2-b]carbazole (FICZ) in vivo are enhanced by loss of CYP1A function in an Ahr2-dependent manner. *Biochemical Pharmacology*. Available at: http://linkinghub.elsevier.com/retrieve/pii/S0006295216300661.

Xiong, K.M., Peterson, R.E. & Heideman, W., 2008. Aryl Hydrocarbon Receptor-Mediated Down-Regulation of Sox9b Causes Jaw Malformation in Zebrafish Embryos. *Molecular Pharmacology*, 74(6), pp.1544–1553.

Appendix A

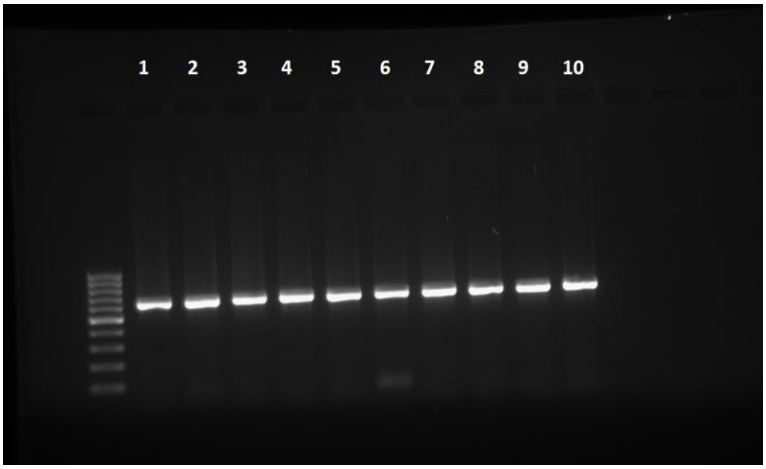

Figure A.1 *– DNA from zebrafish fin clips, amplified with PCR primers AHR2-mut and run on agarose gel with ethidium bromide. Ladder is present in well on furthermost left side and numbers indicate 10 different embryos from ahr2^{hu3335} mutant heterozygous crosses. DNA fragment is supposedly 544 bp long. Ladder: 100 bp, Fermentas.*

Table A-1 *- Primer sequences for PCR experiments. AHR2- mut is obtained from* (Goodale et al. 2012).

Target	Forward primer (5' – 3')	Reverse primer (5' – 3')
AHR2-mut	TATTGCTAGGCAGAGAGCAC	GATGTCTTCTGTGATGATTTCG
Sox9b	GAGTCTGAAGATGGAGAGCAGACG	TAGGGGTGGTGGGTGGTGTG
Cyp1a1	GGATGAAAAGATCGGGAAGGATCG	GGATGTGCAGTGAGGAATGGTG
Foxq1b	GGAGGAGGAATTGGGCTCG	TGTAAGAGTAAG GTGGTTTGGGTCT
Actb1	CGAGCAGGAGATGGGAACC	CAACGGAAACGCTCATTGC
Ppia2	GGGTGGTAATGGAGCTGAGA	AATGGACTTGCCACCAGTTC